Journal of Power Sources 270 (2014) 304–311

Contents lists available at ScienceDirect

Journal of Power Sources

journal homepage: www.elsevier.com/locate/jpowsour

$Li_4Ti_5O_{12}$ coated graphite anodes with piperidinium-based hybrid electrolytes for lithium ion batteries

Kun Gao, Shu-Dan Li*

School of Chemistry and Materials Science, Shanxi Normal University, Linfen 041004, China

HIGHLIGHTS

- $Li_4Ti_5O_{12}$ coated graphite were obtained by a hydrothermal process.
- $Li_4Ti_5O_{12}$ coated graphite were first used in piperidinium-based electrolytes.
- $Li_4Ti_5O_{12}$ coating helps to improve the graphite/electrolyte interfacial stability.
- The modified graphite with 5 wt.% $Li_4Ti_5O_{12}$ revealed excellent cell performances.

ARTICLE INFO

Article history:
Received 2 May 2014
Received in revised form
20 July 2014
Accepted 21 July 2014
Available online 29 July 2014

Keywords:
Lithium-ion battery
Graphite
Lithium titanate
Ionic liquid

ABSTRACT

The electrochemical performances of the 2 wt% and 5 wt% $Li_4Ti_5O_{12}$ coated carbon microbeads (CMB) composites in the piperidinium-based hybrid electrolytes are investigated. Particularly, the interfacial properties and crystal structures of cycled LTO-CMB electrodes are explored by means of scanning electron microscopy, electrochemical impedance and X-ray diffraction. It is found that, the $Li_4Ti_5O_{12}$ coating can help to reduce the interfacial reactions and decrease the initial irreversible capacity. At 0.05 C, the initial coulombic efficiency are improved from 62.7% of pristine CMB to 63.5% of 2% LTO-CMB and 72.5% of 5% LTO-CMB respectively. However, due to its incomplete surface coating, the discharge capacities of 2% LTO-CMB vary with cycle number as an undulate shape, and show a large capacity loss. By contrast, the cycled 5% LTO-CMB covered by a stable and dense granular surface film, shows better rate capability and cycle life. The discharge capacity can always maintain about 290 mAh g^{-1} during the first 22 cycles at 0.1 C. Even at 1 C or 2 C, the reversible capacity is about 50–100 mAh g^{-1} higher than the unmodified CMB.

1. Introduction

Recently, the hybrid electrolytes of ionic liquids (ILs) with organic solvents have aroused strong interest of researchers due to their reasonable ionic conductivity, high chemical and thermal stabilities, and high safety [1–3]. However, there are still some intrinsic barriers to be resolved for the realistic application of graphite anodes with the hybrid electrolytes. (1) Comparatively low charge–discharge capacity. For example, S. F. Lux [4] and B. S. Lalia [5] reported the discharge capacities of graphite/Li cells with 1.0 M LiTFSI-PYR_{14}TFSI-5 wt%VC and 0.4 M LiTFSI-PP_{13}TFSI-10 vol% EC were only 130 and 154.2 mAh g^{-1}, respectively. Moreover, A. Guerfi et al. [6] also found that the first two discharge capacities of MCMB/Li cells using the EMITFSI/50 wt% organic solvent based electrolyte showed 255 and 248 mAh g^{-1} at C/24 rate, which were much lower than that using conventional organic electrolyte. (2) Excessively high electrode/electrolyte interfacial resistance. Recently, A. Lewandowski et al. [7] tested the electrochemical impedance spectra of Li/0.4 M LiTFSI-PP_{13}TFSI-7.5 wt% VC-PVdF-*co*-HFP/Li symmetric cell and found that the interfacial impedance increased from 400 Ω up to 50 kΩ after 47 days of storage. Meanwhile, the discharging capacity of the corresponding graphite/Li half cell dropped from the initial 270 to 120 mAh g^{-1} after 50 cycles at 10 mA g^{-1} rate. (3) Large initial irreversible capacity and fairly poor rate performance. H. Zheng et al. [8] investigated the cycling performance of natural graphite against lithium in 1 M LiTFSI-TMHATFSI-20 vol% EC at 30 °C. During the initial 20 cycles, the discharge capacity dropped rapidly from the initial 330 to 280 mAh g^{-1} at 15 mA g^{-1} rate. And the coulombic efficiency was only increased from 68% to 83.7% for the first three cycles. Y. An et al. [9] also found that in 1.0 M $LiPF_6$-50

* Corresponding author.
E-mail address: lishudan0451@163.com (S.-D. Li).

http://dx.doi.org/10.1016/j.jpowsour.2014.07.133
0378-7753/

vol% $PP_{13}TFSI$-EC/DEC, the first discharge capacity of graphite-hard carbon composite at 0.15 C was only 205 mAh g^{-1}, and coulomb efficiency is only 68%. When the charge–discharge rate increased to 0.3 C, the value of capacity is even lower than 100 mAh g^{-1}. All the above-mentioned problems are closely related to solid electrolyte interphase (SEI). Surface coating may help to improve the interfacial compatibility between carbon electrodes and ILs-based electrolyte.

Lately, the electrochemical performances of $Li_4Ti_5O_{12}$ coated graphite composites in the conventional organic electrolytes have been investigated. The modified graphite could suppress effectively the growth of interfacial resistance and charge-transfer resistance during the prolonged charging–discharging cycles, and decrease greatly the initial irreversible capacity by the reduced interfacial reactions [10]. M. Lu et al. [11] further pointed that the reduced charge transfer resistance could be attributed to the lithiated $Li_4Ti_5O_{12}$ ($Li_7Ti_5O_{12}$ or $Li_9Ti_5O_{12}$) with a higher electronic conductivity, located on the surface of graphite electrode. Even in the case of ILs-based electrolytes, the spinel $Li_4Ti_5O_{12}$ electrodes still behave as well as that in the common organic electrolytes. For example, P. Resl et al. [12] found that $Li_4Ti_5O_{12}$ had the clear redox peaks and flat voltage profiles in 0.2 M LiTFSI-$PYR_{24}TFSI$, which were comparable with that in organic electrolytes. The reversible capacity was close to the 80% of theoretical value at 0.1 C rate, and had no deterioration with cycling. L. Lombardo et al. [13] reported that the full Li-ion cell realized by coupling $LiFePO_4$ and $Li_4Ti_5O_{12}$ electrodes showed stable capacity (about 150 mAh g^{-1}) during the first ten cycles at C/5 rate in 1.0 M $LiPF_6$-EC/DMC-70 wt% $PYR_{14}TFSI$ hybrid electrolyte. Therefore, the $Li_4Ti_5O_{12}$ coating might be beneficial to solve the problems that graphite anodes exist in the ILs-based electrolytes, such as poor electrochemical performance, high interfacial resistance and large initial irreversible capacity, etc.

In our recent work [14], the hybrid electrolytes (0.4 mol kg^{-1} $LiPF_6$-60 wt% $PP_{13}TFSI$-EC/DEC) showed the combined advantages of high ionic conductivity and excellent thermal safety, but the first five discharge capacity of carbon microbeads (CMB) electrode were no more than 180 mAh g^{-1}. The higher interfacial resistance should take partly responsibility for this poor performance. Aim to further improve the electrochemical performance of CMB material, here we prepared the $Li_4Ti_5O_{12}$ coated CMB (LTO-CMB) composites. Their physical properties and electrochemical performances in the piperidinium-based hybrid electrolytes were compared, and then the positive factors and possible mechanism were discussed.

2. Experimental

2.1. Materials

N-methyl-*N*-propylpiperidinium bis(trifluoromethanesulfonyl) ($PP_{13}TFSI$, >99%) was purchased from Shanghai Cheng-Jie Chemical Co., Ltd. The battery-grade ethylene carbonate (EC) and diethyl carbonate (DEC) were obtained from Zhangjiagang Guotai-Huarong New Chemical Materials Co., Ltd. Lithium hexafluorophosphate ($LiPF_6$) was provided from Beijing Ruizhi-Tianxing technology trades Co., Ltd. The carbon microbeads (CMB) materials were supported by Xinxiang Huaxin Energy Materials Co., Ltd.

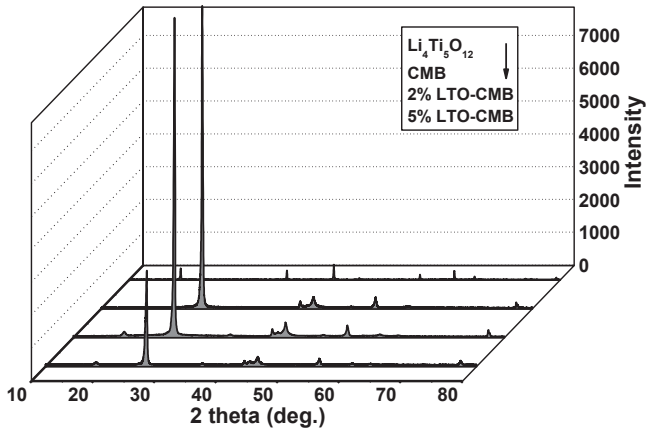

Fig. 2. XRD patterns of pristine CMB, $Li_4Ti_5O_{12}$, 2% and 5% LTO-CMB samples.

2.2. Methods

The schematic of the preparation process of LTO-CMB composite was shown in Fig. 1. The intended $Li_4Ti_5O_{12}$ amounts are 2 wt% and 5 wt% of the total LTO-CMB composites (denoted as 2% and 5% LTO-CMB, respectively). They were prepared via a hydrothermal process followed by a solid-state calcination. Firstly, the pristine CMB powders were pretreated in 63% HNO_3 at 60 °C for 6 h followed by washing with deionized water. Secondly, the stoichiometric amount of tetrabutyl titanate and lithium hydroxide (i.e. Li/Ti = 4:5) were thoroughly mixed in an adequate ethanediol at ambient temperature using a magnetic stirrer in a closed container for about 12 h. Thirdly, the ultrasonic dispersed CMB powders in the water–ethanediol solvent were added into the above salts solution, and the mixture was kept strongly stirring for few minutes. Then, the obtained solution was transferred to a 100 mL Teflon-lined stainless autoclave and stayed in an oven at 180 °C for 36 h. Finally, the powers deposited at the bottom of the reactor were filtered, and dried in oven at 80 °C to remove the residual solvents. To form the LTO-CMB composites, the precursors were heat-treated at 600 °C for 8 h in a vacuum oven.

2.3. Structural characterization

The phases and crystal structures were analyzed by powder *X*-ray diffraction (Ultima IV, Rigaku) employing Cu $K_{\alpha 1}$ radiation

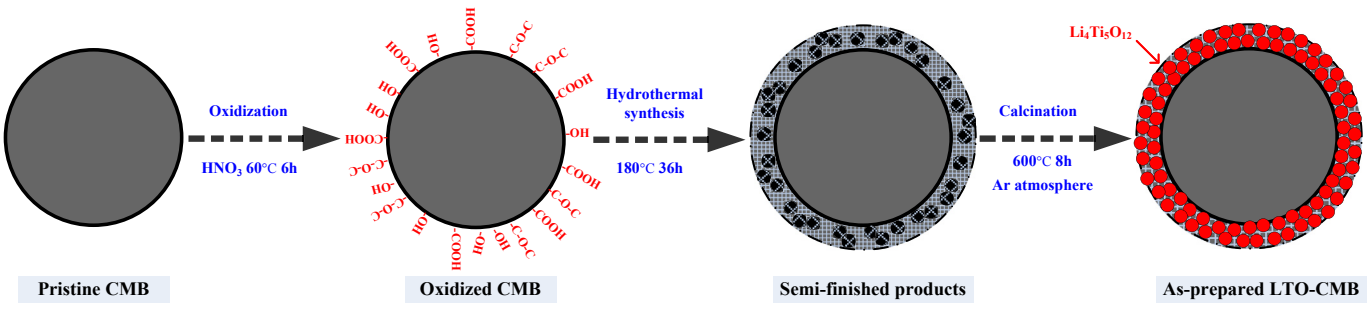

Fig. 1. Schematic illustration of the preparation process of LTO-CMB composite by a hydrothermal method.

(λ = 0.154056 nm) in the two-theta range of 10–80°. The surface morphologies were observed using the scanning electron microscope (SEM, JSM-7500F, Hitachi) equipped with an energy dispersive X-ray analyzer (EDS, Oxford Inca PentaFET × 3). The specific surface area was determined by the aid of BET surface area and pore size analyzer (SA3100, America Beckman Coulter).

2.4. Electrochemical measurement

The hybrid electrolytes were manufactured by the dissolution of 0.7 mol kg^{-1} $LiPF_6$ salt in the $PP_{13}TFSI$ and EC-DEC co-solvents with the mass ratio of 40 wt% and 60 wt%, which was hereafter referred to as 0.7 mol kg^{-1} $LiPF_6$-40 wt% $PP_{13}TFSI$-EC/DEC. The working electrodes consisting of LTO-CMB powders (90 wt%) and polyvinylidene fluoride binder (10 wt%) were first cut into the disks with 16 mm in diameter and further vacuum dried at 100 °C for 12 h. The glass microfiber filter paper with 0.5 mm thickness (Zhangjiagang Tianlei AGM Co., Ltd.) was used as the separator. Subsequently, the CR2025 coin cells were assembled in an argon-filled glove box.

The charge–discharge performances were characterized on a 5 V/2 mA battery testing system (Land 2005A, Wuhan Jinnuo Electronics Co., Ltd.) with cut-off voltage of 0.01–1.5 V *vs.* Li/Li^+ at a constant current from 0.05 C to 2 C. The cells impedance spectra were measured using an electrochemical workstation (CHI 604D, Shanghai CH Instruments, Inc.). The frequency range and voltage amplitude were set from 100 kHz to 0.01 Hz and at 5 mV, respectively.

3. Results and discussion

Fig. 2 compares XRD patterns of pristine CMB, $Li_4Ti_5O_{12}$, 2% and 5% LTO-CMB samples. The pristine CMB shows the typical hexagonal graphite structure, whose main peaks of 2θ are 26.410°, 42.311°, 44.460°, 54.580° and 77.392° (JCPDF No. 41-1487), while the $Li_4Ti_5O_{12}$ sample exhibits the main X-ray diffraction peaks at 18.331°, 35.571°, 43.242°, 57.213°, 62.833° and 66.073°, which can be assigned to a cubic spinel $Li_4Ti_5O_{12}$ with F*d*3*m* space group (JCPDF No. 49-0207). In the case of LTO-CMB composites, the certain distinguishable characteristics of CMB and $Li_4Ti_5O_{12}$ appear at the same time, indicating the two phases coexistence.

Fig. 3 compares the SEM photos of pristine CMB, 2% and 5% LTO-CMB samples. It is easy to see that, compared with the original spherical particles with lightly rough surface, 2% LTO-CMB is partially interspersed with the ribbons, while 5% LTO-CMB is uniformly covered by the thicker shell. From the amplified inset image we can further observe that the $Li_4Ti_5O_{12}$ layer, located on the surface of LTO-CMB samples, actually consists of many tiny and uniform particles. Clearly, 5% LTO-CMB can realize the larger coverage rate than 2% LTO-CMB. To further discover the surface characteristics after $Li_4Ti_5O_{12}$ coating, the EDS comparative tests were carried out at the typical position (point A and B) with significant morphological differences on the surface of 2% LTO-CMB. As expected, the exposed surface (point A) consists largely of carbon, while the area covered by fine powders (point B) presents obvious Ti element. A little oxygen element reasonably come from oxidized graphite and lithium titanate. Based on the above results, the $Li_4Ti_5O_{12}$ phase can be successfully coated on the surface of CMB material by the designed hydrothermal process.

Furthermore, the specific surface area of original CMB was 2.787 m^2 g^{-1}, after coating it increased to 2.841 and 3.085 m^2 g^{-1} for 2% and 5% LTO-CMB, respectively. Obviously, this result was caused by the introduced nano-sized $Li_4Ti_5O_{12}$ with large specific surface area.

Fig. 4 compares the first two charge–discharge curves of the samples with and without $Li_4Ti_5O_{12}$ coating in the hybrid

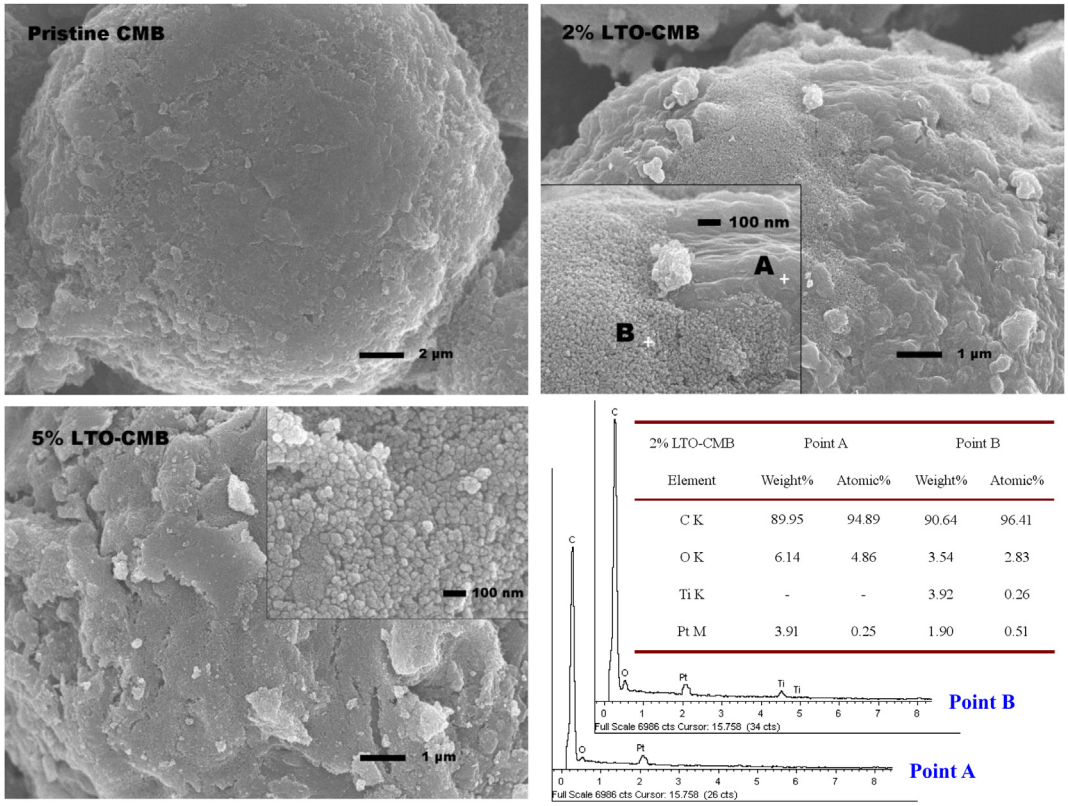

Fig. 3. SEM photographs of pristine CMB, 2% and 5% LTO-CMB and EDS analysis of 2% LTO-CMB.

electrolyte, and the performances of 5% LTO-CMB in organic electrolyte were also shown as a reference. To better observe curve plateaus, the local amplified *dQ*/*dV* curves were embedded into Fig. 4.

Fig. 4a shows that the first charge and discharge capacities of pristine CMB in 0.7 mol kg^{-1} $LiPF_6$-40% $PP_{13}TFSI$-EC/DEC are 438.3 and 274.7 mAh g^{-1}, respectively. The initial coulombic efficiency (CE) is only 62.7%. The large irreversible capacity can be attributed to the CMB/electrolyte interfacial reactions, which mainly include the intercalation of PP_{13}^{+} at around 1.0 V and the decomposition of organic solvents (EC-DEC) between 0.8 V and 0.3 V [5,15–19]. However, the charge capacity at 2nd cycle rapidly decreases to 275 mAh g^{-1} and the corresponding CE increases to 96.5%. The charge–discharge behaviors of oxidized CMB are as same as pristine CMB, such as the first two discharge capacities of 270.8 and 264.6 mAh g^{-1}, and the poor initial CE (65.5%) etc. The both samples without $Li_4Ti_5O_{12}$ showed two main interfacial events of PP_{13}^{+} insertion and EC-DEC decomposition in 1.0 V–0.3 V range during

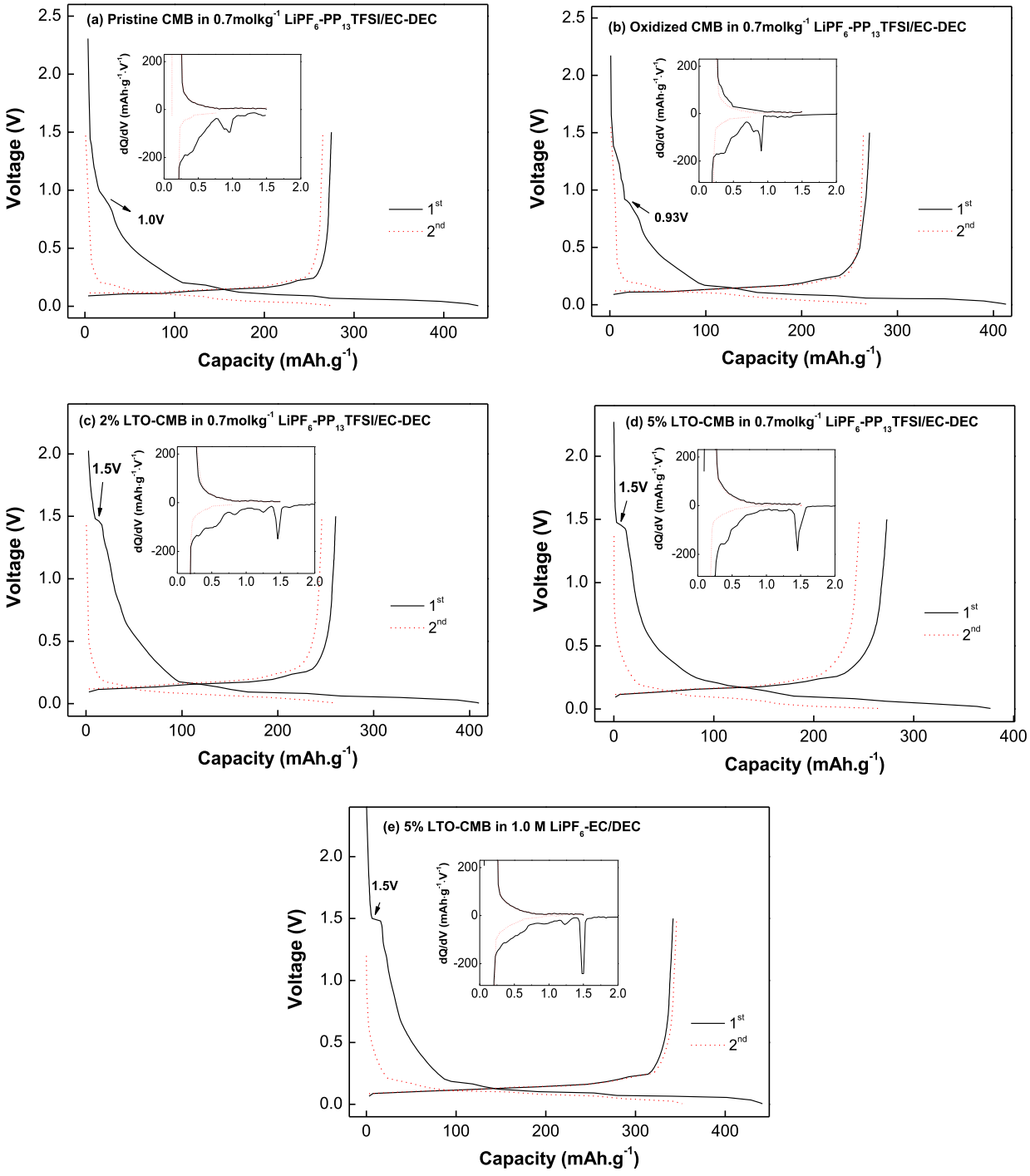

Fig. 4. The first two charge–discharge and amplified differential capacity curves of (a) pristine CMB, (b) oxidized CMB, (c) 2% LTO-CMB, (d) 5% LTO-CMB in 0.7 mol kg^{-1} $LiPF_6$-40% $PP_{13}TFSI$-EC/DEC, and (e) 5% LTO-CMB in 1.0 M $LiPF_6$-EC/DEC.

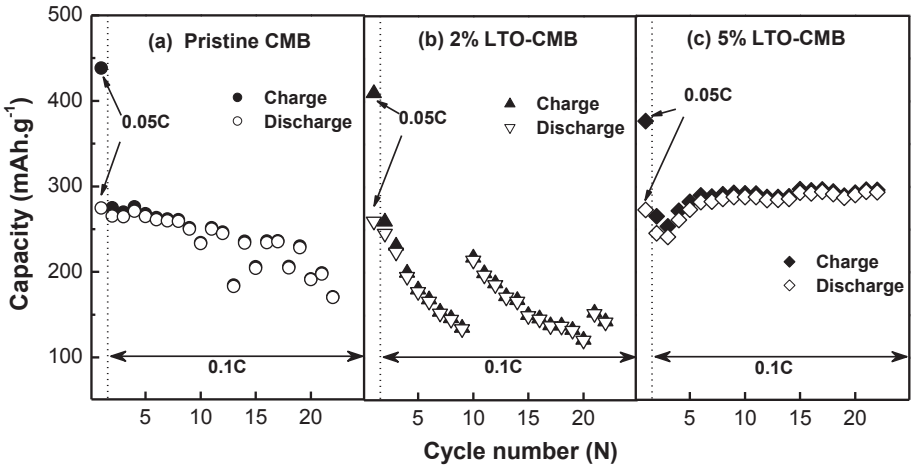

Fig. 5. Cycling performance of CMB, 2% and 5% LTO-CMB in 0.7 mol kg^{-1} $LiPF_6$-40 wt% $PP_{13}TFSI$-EC/DEC.

the first charge, which could be clearly illustrated by theirs *dQ*/*dV* inserts in Fig. 4a and b. But a tiny change is worth to note that the potential of PP_{13}^{+} insertion moved from 1.0 V to 0.93 V after oxidation treatment. Under the same test conditions, the most likely reason for it is the detailed surface variation of oxidized CMB. After being coated with $Li_4Ti_5O_{12}$, the LTO-CMB composites had an obvious charge plateau at around 1.5 V ascribed to the intercalation of Li-ions into $Li_4Ti_5O_{12}$ structure, while the charge plateau at around 1.0 V almost disappears, indicating the impaired intercalation of PP_{13}^{+} cations. These behaviors are very similar to that in organic electrolytes (Fig. 4e), except the capacity decay by the impact of electrolyte viscosity and ionic conduction. The comparison convince that, when CMB is used in the $PP_{13}TFSI$-based electrolyte, $Li_4Ti_5O_{12}$ coating can greatly help to avoid the plague by PP_{13}^{+} insertions. Furthermore, from the magnified inserts in Fig. 4c and d, we can observe that the first differential capacity curves in the zone of 0.8–0.3 V slightly approach the base line with the increasing $Li_4Ti_5O_{12}$. This phenomenon implies that $Li_4Ti_5O_{12}$ coating can also restrain the interfacial decomposition of EC-DEC to some extent. Note that 5% LTO-CMB delivers a maximal first CE of 72.5% in all tested samples with the hybrid electrolyte, while the 63.5% of 2% LTO-CMB is only comparable to that of the samples without $Li_4Ti_5O_{12}$ coating. In fact, for LTO-CMB samples, the initial irreversible capacities partly come from the irreversible Li^+ insertions into $Li_4Ti_5O_{12}$ limited by the cut-off voltage of 0.01–1.5 V. For this reason, the irreversible capacities calculated above are running high. As far as CMB materials are concerned, the actual reversibility gets greatly improved. In addition, the $Li_4Ti_5O_{12}$ coating doesn't seriously affect the subsequent cycles, the typical lithium intercalation/de-intercalation behaviors into/from CMB electrodes can be observed obviously from the subsequent charge–discharge curves. At 2nd cycle, 2% and 5% LTO-CMB show the high discharge capacities of 246.1 and 245.7 mAh g^{-1}, and the corresponding CEs are 94.7% and 92.5%, respectively.

Fig. 5 shows the charge–discharge capacity as a function the cycle number for CMB and LTO-CMB samples. It can be clearly seen from Fig. 5a that the discharge capacities of CMB/Li cell first fade slowly and then fluctuate severely with a serious capacity loss. At last, it drops down to 170.2 mAh g^{-1} and the corresponding capacity retention is 61.9%. In Fig. 5b, 2% LTO-CMB exhibits a more serious capacity loss than pristine CMB, its discharge capacity at 22nd cycle is only 142.3 mAh g^{-1}. Here, the undulate plot should be worth to note. We speculate that the unusual performance should be related to its incomplete surface coating. Because of different surface materials, the interfacial reactions may vary with the different position on the 2% LTO-CMB surface. Therefore, the existing microscopic stresses caused by the non-uniform passivated products (or the released trace gasses) could make the $Li_4Ti_5O_{12}$ layer loose. Then the generated microgap should lead to the larger contact resistance and worsen the cell performance. However, when the $Li_4Ti_5O_{12}$ coating was completely exfoliated, the newly exposed surface should be sufficiently penetrated by the hybrid electrolyte. As a result, the charge–discharge capacity should be improved again. By contrast, benefiting from the more integrated coating, 5% LTO-CMB shows the best charge–discharge performance in three samples. After 22 cycles, the discharge capacity is still 293.8 mAh g^{-1}, which is even higher than the initial capacity of 273.2 mAh g^{-1}.

Fig. 6 compares the discharge capacities of CMB, 2% and 5% LTO-CMB with 0.7 mol kg^{-1} $LiPF_6$-40 wt% $PP_{13}TFSI$-EC/DEC at different rate. Compared with pristine CMB, 2% LTO-CMB shows some slight improvement in rate performances, although the discharge capacities still fluctuate during the first ten cycles. 5% LTO-CMB has the best rate performance, whose specific capacity is around 140 mAh g^{-1} at 1 C, and approaches to 100 mAh g^{-1} even at 2 C, while that of pristine CMB is only 20-30 mAh g^{-1} at 2 C. According

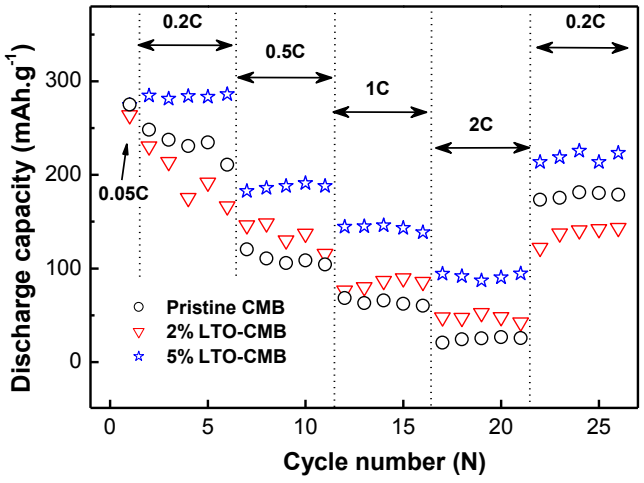

Fig. 6. Rate performances of CMB, 2% and 5% LTO-CMB in 0.7 mol kg^{-1} $LiPF_6$-40 wt% $PP_{13}TFSI$-EC/DEC.

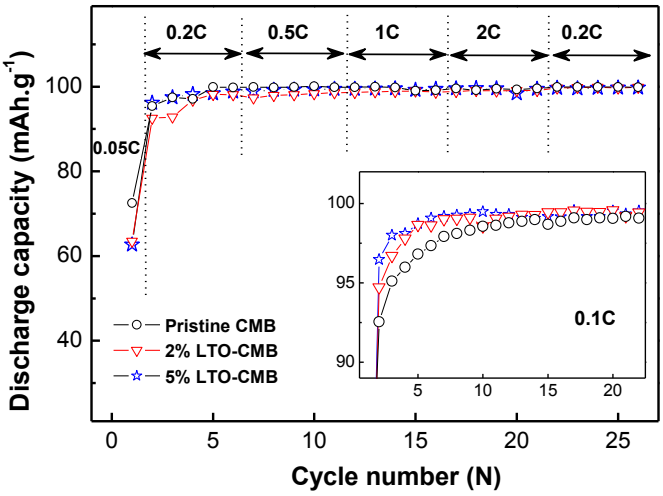

Fig. 7. Coulombic efficiencies (CEs) of CMB, 2% and 5% LTO-CMB at different rate in 0.7 mol kg^{-1} $LiPF_6$-40 wt% $PP_{13}TFSI$-EC/DEC.

to C.Y. Ouyang's report [20], the lithiated $Li_4Ti_5O_{12}$ has a high electronic conductivity similar to metal. This may be an important positive factor for the better rate performances of LTO-CMB composites. Furthermore, when the current density is switched back to 0.2 C in the final test period (22nd–26th), the average capacities of CMB, 2% and 5% LTO-CMB correspond to 76.8%, 71.6% and 77.1% of that in the initial section (2nd–6th), respectively. The result may be caused by the different growth of the interfacial resistance during testing. Here, 5% LTO-CMB exhibits the best capacity recovery.

The effect of different rate on the CEs of CMB, 2% and 5% LTO-CMB in 0.7 mol kg^{-1} $LiPF_6$-40% $PP_{13}TFSI$-EC/DEC is shown in Fig. 7. The low initial CEs of three samples were significantly improved at 2nd cycle, and grew gradually near to 100% in the subsequent several cycles. Note that, at 0.1 C, the CEs of 5% LTO-CMB increase slowest in the three samples. It needs about twelve cycles to achieve a maximum of CE. The fine powders coated on the CMB surface might impede the electrolyte penetration into solid electrode, and prolong the formation of SEI films. However, at 0.2 C, 2% LTO-CMB shows the lowest CEs at the 2nd and 3rd cycles. This result suggests that the interfacial reactions should also be influenced by current intensity. Furthermore, 2% LTO-CMB have slightly lower CEs at 10th and 21st cycle just matching its fluctuant capacities. This observation might further promote the preceding speculation that a renewed surface passivation could occur at the exposed position of the $Li_4Ti_5O_{12}$ layer peeling. Additionally, it also should be pointed out that the CEs of 5% LTO-CMB at 0.1 C grow with the increase of cycling, but the highest values are still less than 99.2% appeared at the 21st cycle. There may be always a few mild interfacial reactions at 5% LTO-CMB/hybrid electrolyte interface.

Fig. 8 shows the surface morphologies of the cycled electrodes. It can be seen that, the cycled CMB has a smooth surface covered by SEI film. In the case of 2% LTO-CMB, the cycles produce much exfoliation from the spherical CMB substrates. This may be the main reason for the fluctuant discharge capacities of 2% LTO-CMB/Li

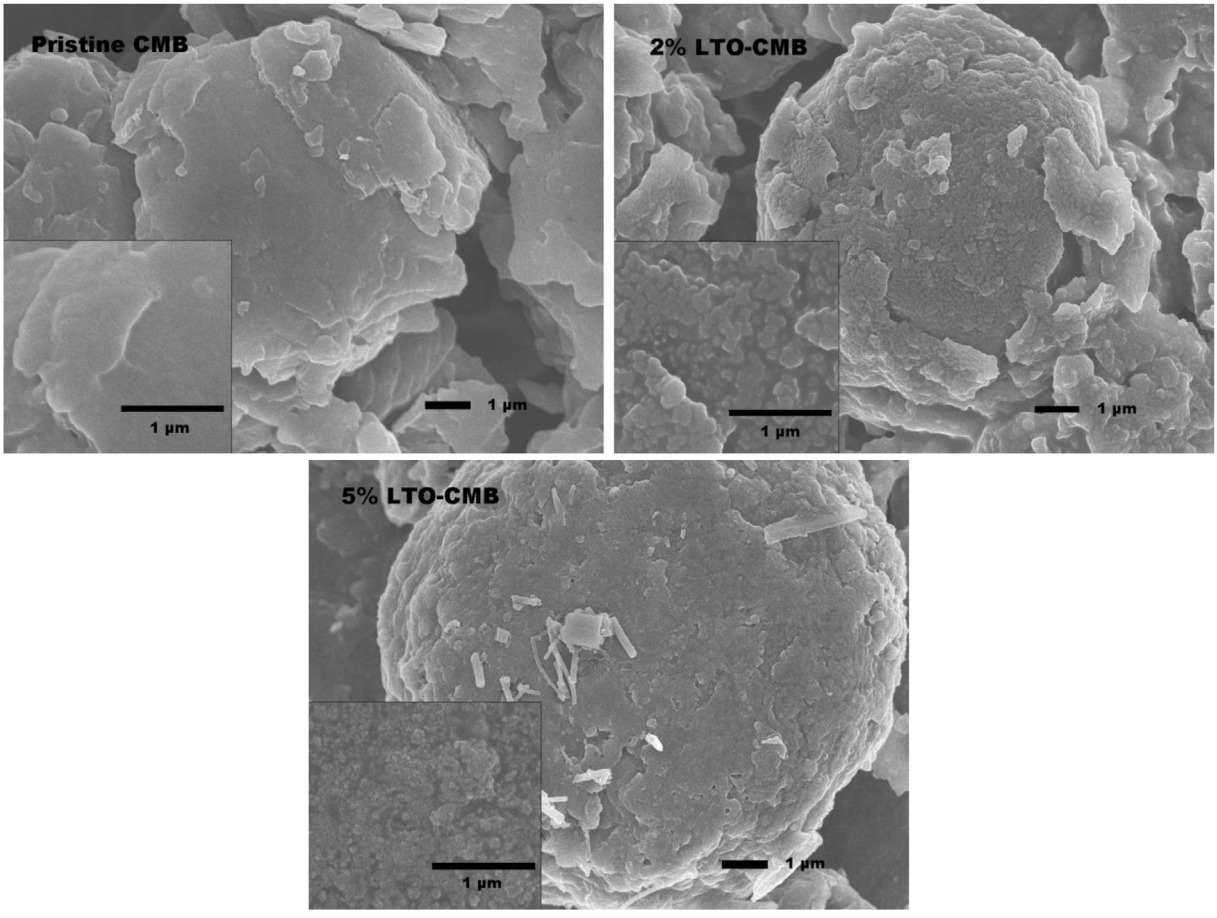

Fig. 8. SEM photographs of the cycled CMB, 2% and 5% LTO-CMB in 0.7 mol kg^{-1} $LiPF_6$-40 wt% $PP_{13}TFSI$-EC/DEC.

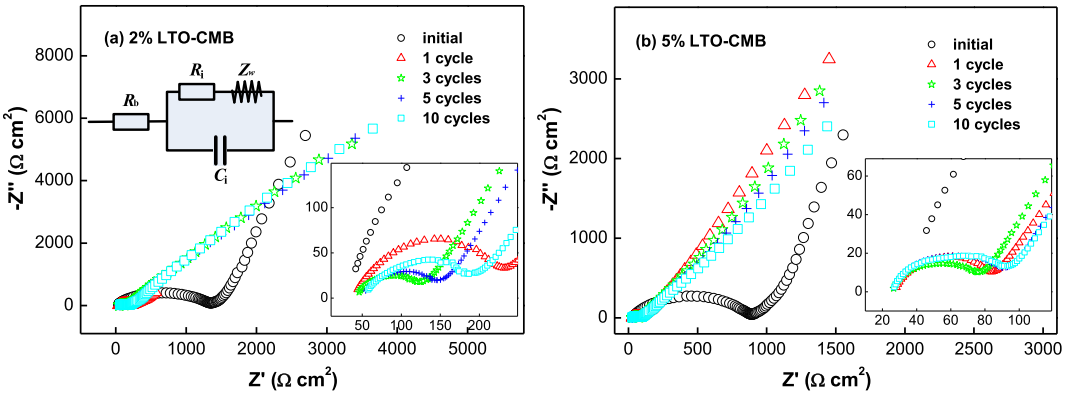

Fig. 9. EIS spectra of 2% (a) and 5% (b) LTO-CMB/Li cells recorded after different cycles.

half cell. On the contrary, the cycled 5% LTO-CMB could almost maintain the integrity of spherical composite. A few strip foreign bodies on the surface are the residual fiberglass separators. In the magnified images, the previous loose $Li_4Ti_5O_{12}$ granules on the surface of un-cycled LTO-CMB composites were closely linked together, and formed a compact SEI shell.

As shown in Fig. 9, the recorded Nyquist spectra of LTO-CMB/Li half cells comprise of one semicircle in high frequencies and a subsequent inclined line at the low frequency end. Here, we employed a simple equivalent circuit embedded in Fig. 9a to model the sole semicircle behaviors [6,21]. In the circuits, R_b is the bulk electrolyte resistance. R_i is the interfacial resistance. C_i is the interfacial capacitance and Z_w is *Warburg* resistance. The fitting data were listed in Table 1. It shows that the LTO-CMB/Li cells both present much large initial R_i values (1027 and 702 Ω cm^2), which can be mainly attributed to theirs poor wetting between liquid electrolyte and solid electrodes for fresh cells. After the initial cycle, the R_i values descended rapidly to 146.6 and 34.71 Ω cm^2 for 2% and 5% LTO-CMB cells, respectively. Meanwhile, the R_b values also has a slightly decline. These phenomena should especially benefit from solid electrode wetting improvement. Throughout the testing process, 2% LTO-CMB/Li cell gave the minimum values of R_b and R_i at the 3rd cycle and then increased with increasing cycles, reflecting the interfacial instability. It is worth to note that, due to the use of 2-electrode coin-cells, the recorded Nyquist plots will be the sum of the impedances of both electrodes (anode and cathode). However, because other factors are not changed, the occurred significant differences in EIS data of both cells can be mainly attributed to the alteration of 2% LTO-CMB and 5% LTO-CMB electrodes. By comparison, the 5% LTO-CMB/Li cell has more stable and lower interfacial impedance. This conclusion can be also used to explain why 5% LTO-CMB shows excellent cycle ability and rate performance.

Fig. 10 compares the XRD patterns of the cycled CMB and LTO-CMB composites. Theirs mean interlayer spacing, d_{002}, can be evaluated from the position of the (002) peak applying *Bragg's* equation. The average crystallite sizes along the *c*-axis, L_c, and the *a*-axis, L_a, can be determined by using the *Scherer* formula from the full-width half-maximum (*FWHM*) of the 002 and 101 peaks with values of $K = 0.89$ for L_c and 1.84 for L_a [22]. These corresponding structural data were presented in Table 2. From Fig. 10, it is easy to see that no obvious diffraction peaks related to $Li_4Ti_5O_{12}$ phase can be observed for the cycled LTO-CMB. Some scholars considered $Li_4Ti_5O_{12}$ should be transferred into amorphous phase ($Li_{8.5}Ti_5O_{12}$) to some extent when charged to 0 V, and only showed few or some weaker diffraction peaks [23]. Furthermore, several differences of XRD patterns are worth to note. (1) The weak peak at around $2\theta = 21°$ related to the PP_{13}^+/CMB intercalation compound [24,25], disappeared after $Li_4Ti_5O_{12}$ modification. (2) The cycled LTO-CMB composites only showed more mild changes in L_c and L_{a101}, and maintained superior graphitization (Table 2). Especially, the G value of 5% LTO-CMB is 94.8% very close to the 95.3% of pristine CMB before cycling. (3) The lower I_{101}/I_{100} values for the cycled LTO-CMB samples imply that the turbostratic structure in pristine CMB material partially turn to order structure because of the shuttle function of Li-ions [26]. These XRD observations further prove that $Li_4Ti_5O_{12}$ coating can help to suppress the intercalation of PP_{13}^+ cations and maintain the more integrated crystal structure.

Table 1
Fitting results from EIS data of 2% and 5% LTO-CMB/Li cells.

Test condition	2% LTO-CMB		5% LTO-CMB	
	R_b (Ω cm^2)	R_i (Ω cm^2)	R_b (Ω cm^2)	R_i (Ω cm^2)
Fresh cell	57.33	1027	61.47	702.3
After 1 cycle	52.76	146.6	30.9	34.71
After 3 cycles	48.68	47.27	28.97	29.41
After 5 cycles	57.57	56.77	29.61	40.04
After 10 cycles	64.47	81.21	30.45	40.05

4. Conclusion

The LTO-CMB composites have been successfully synthesized via a hydrothermal process. When the designed covering amount of

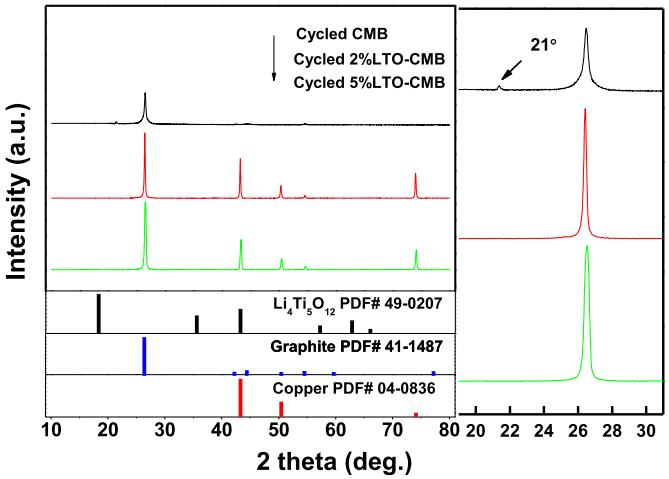

Fig. 10. XRD patterns of the cycled CMB, 2% and 5% LTO-CMB electrodes in 0.7 mol kg^{-1} $LiPF_6$-40 wt% PP_{13}TFSI-EC/DEC.

Table 2
Structure parameters of cycled electrodes calculated from XRD data.

Samples	d_{002} (nm)	G (%)	L_c (nm)	L_{a101} (nm)	I_{101}/I_{100}
Pristine CMB [14]	0.3358	95.3	33.49	35.09	1.83
Cycled CMB [14]	0.3363	89.5	28.51	24.69	2.8
Cycled 2% LTO-CMB	0.3371	80.3	38.06	39.86	1.5
Cycled 5% LTO-CMB	0.3359	94.8	24.99	36.94	1.5

$Li_4Ti_5O_{12}$ is 5 wt%, the final product shows good coating uniformity and surface coverage. The advantages of LTO-CMB composites in term of electrochemistry can be concluded as follows: (1) $Li_4Ti_5O_{12}$ shell can effectively decrease the initial irreversible capacity loss of CMB electrodes by restraining the co-intercalation of PP_{13}^{+} cations and the interfacial reaction of EC-DEC solvents. (2) The lithiated $Li_4Ti_5O_{12}$ has a high electronic conductivity similar to metal and can significantly enhance the cells performances including the rate and cycle ability. (3) The cycled 5% LTO-CMB formed a compact SEI film with granulated structure, showed low resistance as well as high stability, and protected the inner structure effectively. Therefore, the $Li_4Ti_5O_{12}$ coated CMB materials (LTO-CMB) are helpful to improve the electrochemical performances of graphite anodes in the piperidinium-based hybrid electrolytes, and can promote to realize the commercial application of power sources with ILs electrolytes.

Acknowledgments

This work was financially supported by National Natural Science Foundation of China (NSFC) (grant no. 21003087) and Program for the Top Young Academic Leaders of Higher Learning Institutions of Shanxi (TYAL).

References

[1] I. Quinzeni, S. Ferrari, E. Quartarone, C. Tomasi, M. Fagnoni, P. Mustarelli, J. Power Sources 237 (2013) 204.
[2] M. Wang, Z. Shan, J. Tian, K. Yang, X. Liu, H. Liu, K. Zhu, Electrochim. Acta 95 (2013) 301.
[3] S.Y. Bae, E.G. Shim, D.W. Kim, J. Power Sources 244 (2013) 266.
[4] S.F. Lux, M. Schmuck, G.B. Appetecci, S. Passerini, M. Winter, A. Balducci, J. Power Sources 192 (2009) 606.
[5] B.S. Lalia, N. Yoshimoto, M. Egashira, M. Morita, J. Power Sources 195 (2010) 7426.
[6] H. Nakagawa, Y. Fujino, S. Kozono, Y. Katayama, T. Nukuda, H. Sakaebe, H. Matsumoto, K. Tatsumi, J. Power Sources 174 (2007) 1021.
[7] A. Lewandowski, A. Swiderska-Mocek, L. Waliszewski, Electrochim. Acta 92 (2013) 404.
[8] H. Zheng, G. Liu, V. Battaglia, J. Phys. Chem. C 114 (2010) 6182.
[9] Y. An, P. Zuo, X. Cheng, L. Liao, G. Yin, Electrochim. Acta 56 (2011) 4841.
[10] M.L. Lee, Y.H. Li, S.C. Liao, J.M. Chen, J.W. Yeh, H.C. Shih, Appl. Surf. Sci. 258 (2012) 5938.
[11] M. Lu, Y. Tian, X. Zheng, J. Gao, B. Huang, J. Power Sources 219 (2012) 188.
[12] P. Reale, A. Fernicola, B. Scrosati, J. Power Sources 194 (2009) 182.
[13] Lombardo, S. Brutti, M.A. Navarra, S. Panero, P. Reale, J. Power Sources 227 (2013) 8.
[14] K. Gao, X.H. Song, Y. Shi, S.D. Li, Electrochim. Acta 114 (2013) 736.
[15] G.B. Appetecchia, M. Montanino, A. Balducci, S.F. Lux, M. Winterb, S. Passerinia, J. Power Sources 192 (2009) 599.
[16] M. Nádherná, J. Reiter, J. Moskon, R. Dominko, J. Power Sources 196 (2011) 7700.
[17] J. Reitera, M. Nádhernáb, R. Dominko, J. Power Sources 205 (2012) 402.
[18] H.H. Zheng, B. Li, Y.B. Fu, T. Abe, Z. Ogumi, Electrochim. Acta 52 (2006) 1556.
[19] P. Isken, C. Dippel, R. Schmitz, R.W. Schmitz, M. Kunze, S. Passerini, M. Winter, A. Lex-Balducci, Electrochim. Acta 56 (2011) 7530.
[20] C.Y. Ouyang, Z.Y. Zhong, M.S. Lei, Electrochem. Commun. 9 (2007) 1107.
[21] K. Kim, Y.H. Cho, H.C. Shin, J. Power Sources 225 (2013) 113.
[22] I. Cameán, P. Lavela, J.L. Tirado, A.B. García, Fuel 89 (2010) 986.
[23] T.F. Yi, Y. Xie, Y.R. Zhu, R.S. Zhu, H. Shen, J. Power Sources 222 (2013) 448.
[24] V. Baranchugov, E. Markevich, G. Salitra, D. Aurbach, Guenter Semrau, Michael A. Schmidt, J. Electrochem. Soc. 155 (2008) A217.
[25] H. Zheng, K. Jiang, T. Abe, Z. Ogumi, Carbon 44 (2006) 203.
[26] D. Aurbach, H. Teller, E. Levi, J. Electrochem. Soc. 149 (2002) A1255.